An active imaging system using a deformable mirror and its application to super resolution

Deokhwa Hong*[a], Xiaodong Tao[a], Hyungsuck Cho[a]
[a]Korea Advanced Institute of Science and Technology, 373-1 Kuseong Dong, Yuseong Gu, Daejeon, Korea.

ABSTRACT

In this paper, we propose an active vision system which has variable PSF. The system consists of a deformable mirror, an aperture stop and four lenses. The deformable mirror is placed at the pupil plane and its effective size is determined by the aperture stop at the conjugate position of the mirror. We try to enhance the image resolution using this system. We make four different mirror surface shapes to take four regularly shifted images and use super-resolution algorithm to synthesize higher resolution image from the low resolution observations. It is demonstrated that our method can be used to enhance image resolution which is limited by CCD cell size. We compare the result with the real image and some discussion about algorithmic parameters follows.

Keywords: deformable mirror, super-resolution, restoration, active imaging

1. INTRODUCTION

1.1 The active imaging system

A PSF (Point Spread Function), which specifies the characteristics of an optical system, is normally fixed due to fixed composition of the optical components. However, if we can make an optical system have a variable PSF, many interesting applications would be made. One way to make this kind of optical system is to lay an active component, so called, spatial light modulator in the pupil plane so that it can modulate wavefront of incoming light. There are several types of spatial light modulators such as LC-SLM (Liquid Crystal Spatial Light Modulator), AOD (Acousto-Optic Deflector), DMD (Digital Micromirror Device) and deformable mirror[1]. Vincent Laude proposed twisted-nematic liquid-crystal pixilated active lens[2] which has LC-SLM in the pupil plane. In that paper, Laude analyzed characteristics of the active lens and demonstrated phase images on the LC-SLM for basic functionalities such as transversal image shift and focal length change. However, although an LC-SLM provides pixel level phase control in limited range so that one can modulate incoming wave front with very high degree of freedom, there are several inherent problems to be used in general cases[2]. First, because the system is based on refractive index modulation, chromatic aberration should appear. Second, because of the pixelated nature of LC-SLM, high order diffraction rays degrade the image quality. Third, due to complicated combination of aliasing and quantization, ghost image appears to corrupt the image.

We propose an active imaging system which uses a deformable mirror in the pupil plane instead of LC-SLM to avoid these problems. A mirror does not suffer from chromatic aberration, and continuous mirror surface does not cause the troublesome diffraction problem. Furthermore, there is no ghost image, either. Main inferior points of the deformable mirror to LC-SLM are limited capability of controlling wave front. We can not control the surface shape pixel by pixel as one can do with LC-SLM. Only tens of actuators are attached at the backside of the deformable mirror and they are coupled by membrane mirror. Moreover, the deformation of the mirror surface is also very limited. But for simple manipulations, like focus control, image shift or low order aberration compensation, we do not need very complicated mirror shape and large deformation. Therefore, when we consider only small variation of optical system characteristics, using deformable mirror can be a better solution for wavefront manipulation.

In our system, the active component, deformable mirror is placed in the pupil plane and modulates incoming wavefront. We place it at the conjugate position of the aperture stop of the system. Rays that reach the deformable mirror are reflected and go into the imaging system. The required input voltages to get desired mirror surface are calibrated using laser and wave front sensor with reference mirrors in feedback loop and the influence matrix is obtained by experiment.

Optomechatronic Sensors, Instrumentation, and Computer-Vision Systems,
edited by Yasuhiro Takaya, Jonathan Kofman, Proc. of SPIE Vol. 6375
637503, (2006) · 0277-786X/06/$15 · doi: 10.1117/12.686624

1.2 Super resolution

As one possible application of the proposed system, image resolution method using the deformable mirror is shown in this paper. There have been many trials to enhance the image resolution which is limited by CCD cell size, because the size of a CCD cell has physical lower limit due to shot noise, and designing an optical system which is free of aberration for the whole large field is usually difficult and expensive[]. Many research efforts are focused on reconstructing high resolution image, given multiple slightly different low resolution images. Usually the relative motions between the images are unknown in advance, so motion estimation, i.e., registration is one of the most important topics in that area. There are several kinds of approaches proposed, and the recent issues and techniques of super-resolution are summarized and reviewed in [3].

On the other hand, some researchers tried to actively get several displaced images to reconstruct high resolution image. Poletto mounted a mirror on translation stage to get subpixel shifted images by moving the mirror[4], and Vincent Laude used phase image on LC-SLM[5]. In this case, the registration process, whose computational cost is high, is unnecessary because the relative motions between the observations are readly known. However, mounting a mirror on a translational stage can be used to nothing else, and image shifting method using LC-SLM suffers from several problems described above.

In this paper, we use deformable mirror to obtain a synthesize image with enhanced resolution. Using deformable mirror to shift the image position has some advantages against the other methods mentioned above, because it is also applicable to other tasks such as focusing or dynamic aberration correction, and the quality of the image reflected by the continuous mirror surface is better than that of image formed by pixelated LC-SLM. The focal point shifting ability of a deformable membrane mirror was briefly mentioned in [6]. We first calculate the influence matrix of the deformable mirror and use it to calculate the required control signals to shift the image. For reconstruction algorithm, we referred to Rajan's method[7], which uses an optimization method to synthesize a high resolution image from blurred, noisy low resolution images.

In the next section, we show our proposed active vision system. In section 3, we briefly explain the super-resolution algorithm. Section 4 presents experimental results, and conclusions are given in section 5.

2. ACTIVE VISION SYSTEM

2.1 System configuration

The proposed active vision system is shown in Fig.1. The imaging system consists of four lenses, an aperture stop, CCD camera and the deformable mirror. We use 15mm electrostatically driven MMDM (micromachined membrane deformable mirror) from Oko technology which has 37 channels. Because only attractive force is available at each actuator in the deformable mirror, the mirror is used in biased mode. Due to the boundary effect, the effective area of the deformable mirror is less than 10 mm. The detailed structure of an MMDM and the biased mode is well explained in [8], and discussion about actuator arrangement and the optimum effective area of the mirror surface can be found in [9].

Light from one point of the object first passes the lens L1 and is reflected by the deformable mirror to be collimated. It is imaged at the first image plane by L2 and the image is relayed to the image plane by L3 and L4. The aperture stop is at the conjugate position of the deformable mirror and determines the effective area of the deformable mirror, which is about 9~10mm. This configuration makes the deformable mirror able to modulate the incoming light at the pupil plane. The magnification of the system is one, and the pixel size of the camera in the system is $8.4 \times 8.4 \mu m^2$.

2.2 Deformable mirror

The deformable mirror surface can be represented by Zernike polynomials. The detail explanation about Zernike polynomial is available in [10]. We can calibrate the deformable mirror by calculating the influence matrix which relates the input signals to each channel to the mirror deformation[11]. The detailed method to calculate the influence matrix is given in [11]. If $\mathbf{A}$ is the influence matrix, $\mathbf{z}$ is the coefficient vector of the Zernike polynomials and $\mathbf{v}$ is the control signal vector, the relationship between those variables can be represented by Eq.1.

$$\delta \mathbf{z} = \mathbf{A} \delta \mathbf{v} \tag{1}$$

where δ means deviation from the reference.

Once we get the influence matrix, we can calculate the required voltages, given the desired deformation in terms of Zernike polynomials, by multiplying the pseudo inverse of the influence matrix **A** to both sides. In our case, the control signal is from -1 to 1 and we used first 20 terms of Zernike polynomials except the zeroth order term, piston. We obtained the influence matrix by experiment. The Zernike polynomials used in this paper are denoted in Table 1.

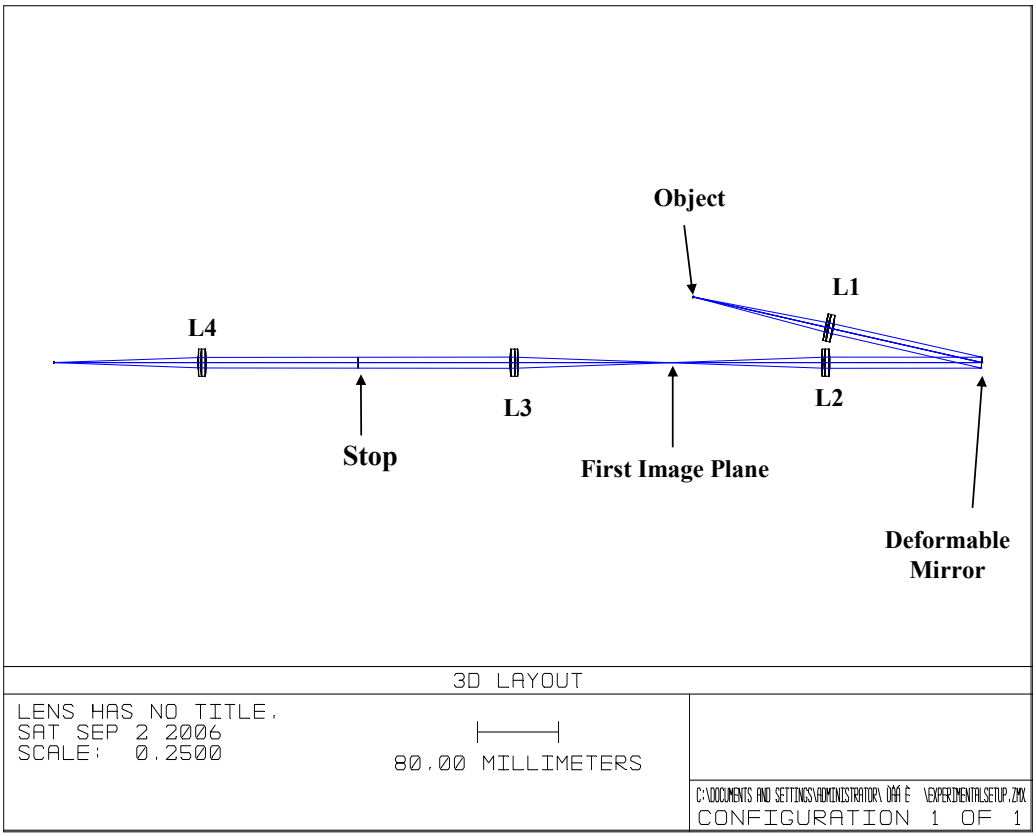

Fig. 1. System configuration

Table 1.the first 20 Zernike polynomials used in this paper

No	Zernike Polynomial	No	Zernike Polynomial	No	Zernike Polynomial	No	Zernike Polynomial
1	$\rho\cos\varphi$	6	$(3\rho^3-2\rho)\cos\varphi$	11	$(4\rho^4-3\rho^2)\cos 2\varphi$	16	$(10\rho^5-12\rho^3+3\rho)\sin\varphi$
2	$\rho\sin\varphi$	7	$(3\rho^3-2\rho)\sin\varphi s$	12	$(4\rho^4-3\rho^2)\sin 2\varphi$	17	$(5\rho^5-4\rho^3)\cos 3\varphi$
3	$2\rho^2-1$	8	$\rho^3\cos 3\varphi$	13	$\rho^4\cos 4\varphi$	18	$(5\rho^5-4\rho^3)\sin 3\varphi$
4	$\rho^2\cos 2\varphi$	9	$\rho^3\sin 3\varphi$	14	$\rho^4\sin 4\varphi$	19	$\rho^5\cos 5\varphi$
5	$\rho^2\sin 2\varphi$	10	$6\rho^4-6\rho^2+1$	15	$(10\rho^5-12\rho^3+3\rho)\cos\varphi$	20	$\rho^5\sin 5\varphi$

3. SUPER RESOLUTION ALGORITHM

In this section, we will briefly introduce the super resolution algorithm. The detailed description of the imaging model and the super-resolution algorithm is available in [12] and [7], respectively.

3.1 Imaging Model

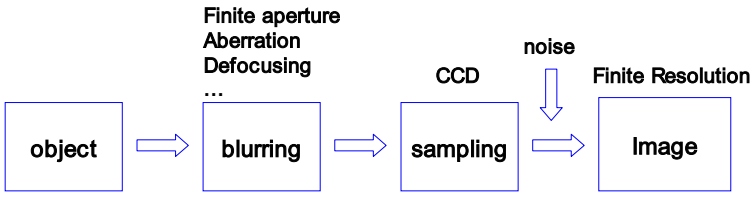

a. Block diagram of general imaging process

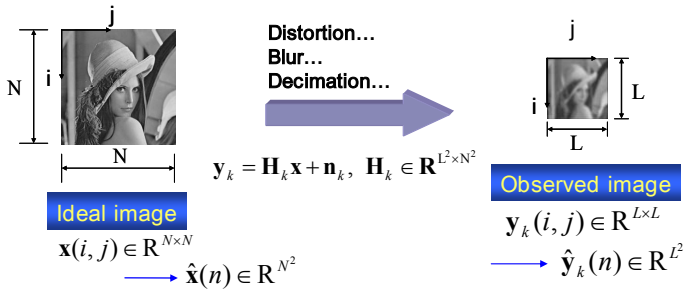

b. Mathematical model of imaging process

Fig. 2. Imaging model

When we image an object through an optical system, light emitted from one point on the object experiences blurring before reaching the image plane due to finite size of the aperture, existing aberration, etc. CCD laid at the image plane samples the image, introducing some more degradation of the image due to finite size of the sensing element and inevitable noise. And finally, we get digitized image from the camera. This process is illustrated in Fig.2a. A super-resolution algorithm attempts to extract the high-resolution image corrupted by those kinds of limitations of the optical imaging system.

Making an appropriate mathematical imaging model helps us formulating the super-resolution problem. We denote a 2D image by its vectorized form. As shown in Fig.2b, suppose that there is an ideal high resolution $N \times N$ image denoted by $\mathbf{x} \in R^{N^2}$, which is degraded and decimated to be $\mathbf{y}_k \in R^{L^2}$ by a factor of M, i.e.,

$$M = \frac{M}{L}. \tag{2}$$

We call the sampled image $\mathbf{y}_k$ an observation. We can relate the ideal high resolution image $\mathbf{x}$ to an observation $\mathbf{y}_k$ by $\mathbf{H}_k$ which incorporates blurring and decimation as the following equation,

$$\mathbf{y}_k = \mathbf{H}_k \mathbf{x} + \mathbf{n}_k, \ \mathbf{H}_k \in \mathbf{R}^{L^2 \times N^2} \tag{3}$$

where $\mathbf{n}_k$ represents the sensor noise.

Now, super-resolution becomes an inverse problem as described in Fig.3. We should estimate the high resolution image $\mathbf{x}$ from the observation $\mathbf{y}_k$'s, assuming that $\mathbf{H}_k$ is known. Due to the ill-posedness of the problem, we need to have several observations. Each observation will constitute Eq.3, and by stacking them, we can build Eq.4, as follows:

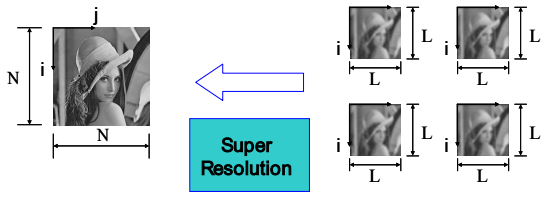

Fig. 3. Basic concept of the super-resolution

$$\mathbf{y} = \mathbf{H}\mathbf{x} + \mathbf{n}, \ \ \mathbf{H} \in \mathbf{R}^{KL^2 \times N^2} \tag{4}$$

where,

$$\mathbf{y} = \begin{bmatrix} \mathbf{y}_1 \\ \mathbf{y}_1 \\ \vdots \\ \mathbf{y}_p \end{bmatrix} \tag{5}$$

and

$$\mathbf{H} = \begin{bmatrix} \mathbf{H}_1 \\ \mathbf{H}_1 \\ \vdots \\ \mathbf{H}_p \end{bmatrix}. \tag{6}$$

For $\mathbf{H}$ to be nonsingular, we need at least M^2 different observations or regularizing method[3].

3.2 Super resolution algorithm

By using the imaging model, the problem seems to be reduced to simple matrix manipulation, but that is not the case. Calculating the inverse or pseudo inverse of $\mathbf{H}$ is not a trivial task because usually the size of $\mathbf{H}$ is very large. Moreover, because $\mathbf{H}$ is highly sensitive to noise, we can not obtain an acceptable result by simply calculating the inverse even in the presence of very small noise. There have been many approaches to solve this problem, which are well summarized in [3]. In this paper, we referred to Rajan's MRF-Based Approach [7] to reconstruct high resolution image from blurred, noise observations.

In [7], super-resolution problem is cast onto the restoration frame work. The reconstructed high resolution image is regarded as an MRF (Markov Random Field), and MAP (Maximum A Posteriori) estimation technique is used to obtain the high resolution image $\mathbf{x}$, given the observation $\mathbf{y}_k$'s, i.e.,

$$\begin{aligned} \hat{\mathbf{x}} &= \arg\max_{\mathbf{x}} P(\mathbf{x} \mid \mathbf{y}_1, \mathbf{y}_2, ..., \mathbf{y}_p) \\ &= \arg\min_{\mathbf{x}} \left\{ \sum_{k=1}^{P} \frac{\left\| \mathbf{y}_k - \mathbf{H}_k \mathbf{x} \right\|^2}{2\sigma_\eta^2} + V(\mathbf{x}) \right\} \end{aligned} \tag{7}$$

where σ_η^2 denotes the variance of the noise process and $V(\mathbf{x})$ is a description of contextual constraints. We can use smoothness constraint by imposing a quadratic cost the difference of intensity values between neighboring pixels as Eq.8.

$$V(\mathbf{x}) = \frac{1}{\lambda} \sum_{i=1}^{N_1} \sum_{j=1}^{N_2} \left[\left(\mathbf{x}(i,j) - \mathbf{x}(i,j-1) \right)^2 + \left(\mathbf{x}(i,j) - \mathbf{x}(i-1,j) \right)^2 \right] \tag{8}$$

where λ can be thought as a tuning parameter. As λ decreases, the resultant image gets more smoothened. Using this constraint ensures the convexity of the overall objective function so that we can use simple gradient descent method to find the optimum image $\mathbf{x}$. This objective function surely abates the effect of noise by regularizing the resultant image, but it also smoothens meaningful discontinuities in the image. To avoid this problem, one can incorporate line field in the cost to preserve discontinuities as Eq.9.

$$\begin{aligned} V(\mathbf{x}) = \sum_{i,j} \frac{1}{\lambda} [&(x_{i,j} - x_{i,j-1})^2 (1 - v_{i,j}) + (x_{i,j+1} - x_{i,j})^2 (1 - v_{i,j+1}) \\ &+ (x_{i,j} - x_{i-1,j})^2 (1 - l_{i,j}) + (x_{i+1,j} - x_{i,j})^2 (1 - l_{i+1,j})] \\ &+ \alpha [l_{i,j} + l_{i+1,j} + v_{i,j} + v_{i,j+1}] \end{aligned} \tag{9}$$

$$v_{i,j} = \begin{cases} 1, & if \ \left| x_{i,j} - x_{i,j-1} \right| \geq h_0 \\ 0, & otherwise \end{cases}, \quad l_{i,j} = \begin{cases} 1, & if \ \left| x_{i,j} - x_{i-1,j} \right| \geq h_0 \\ 0, & otherwise \end{cases} \tag{10}$$

v and l denotes the horizontal and vertical line fields, which are, as defined in Eq.10, one if the difference of the intensity values between neighboring pixels is greater than a given value h_0, or zero, otherwise. h_0 can be regarded as a threshold value or contrast sensitivity. By checking whether intensity difference between neighboring pixels exceeds h_0 or not, one can determine weather the discontinuity under inspection is meaningful or not. When a linefield $v_{i,j}$ or $l_{i,j}$ is one, i.e., the horizontal or vertical discontinuity at point (i, j) is thought to be meaningful, the intensity difference does not contribute the smoothness cost as we can see in Eq.9.

Line field of the optimized image depends not only on h_0 but also on λ. Isolation between discontinuities is determined by the characteristic length L_c which is,

$$L_c = \frac{1}{\sqrt{\lambda}} \tag{11}$$

When two adjacent discontinuities are closer than L_c, the contrast sensitivity is no more h_0 but increases. One more consideration we have to take to use this discontinuity preserving algorithm is gradient limit. We can define another parameter gradient limit g_l from those two parameters as,

$$g_l = \frac{1}{2} h_0 \sqrt{\lambda} \tag{12}$$

When gradient at a point exceeds g_l line field at the point becomes one.

We cannot directly use simple gradient descent algorithm to obtain the optimum image because incorporating line field to cost function does not ensure the convexity of the overall objective function. We have to use GNC algorithm instead. The detailed explanation about line field generation and GNC algorithm can be found in [13].

4. EXPERIMENTS

4.1 The desired mirror shape for super-resolution reconstruction

In [7], they claim that they could reconstruct a higher resolution image without any relative motion between the sampled images, but we found that the performance of super-resolution algorithm with motionless samples is not comparable to that of the method which uses observations having relative motions each other. Therefore, we will try to get four regularly shifted samples, among which is one reference image and are thee shifted images from the reference in horizontal, vertical and diagonal directions, and use them to reconstruct a higher resolution image.

To obtain four relatively shifted images, we should know the desired shape of the deformable mirror for each sample. Because image shift is related to the first order Zernike polynomial terms, tip and tilt, we tried to get the appropriate

coefficients corresponding to those terms using a ray tracing software, Zemax. The deformable mirror surface is simulated by 'Zernike Standard Sag' surface. Because the mirror is operating in biased mode, the initial shape of the deformable mirror is convex whose radius of curvature is -5m . We call this shape a reference shape. We found that $0.05\,\mu m$ change of coefficients of the first order polynomial terms induces $12\,\mu m$ spot shift in the image plane. Because the pixel size of the camera is $8.4\times 8.4\mu m^2$, we need to change the coefficient of the first order Zernike polynomial term $0.35\,\mu m$ to shift the spot position by one pixel size. Fig.4 shows the reference shape (Fig.4a) and change of the mirror surface when we add nothing (Fig.4b), tip (Fig.4c), tilt (Fig.4d), both tip and tilt (Fig.4e) of amplitude $0.5\,\mu m$ to the reference shape. In the figure, the radius of the mirror is normalized to one. The mirror shapes are denoted by intensity variation, where the deeper area is darker. Unit of depth is millimeter. We can see that when we add tip or tilt term to the mirror surface, the deepest point deviates from the center point in vertical, horizontal and diagonal direction, respectively.

The curvature of the mirror surface may be different from time to time because the reference mirror shape can not be exactly -5m and sometimes the deformable mirror should change its curvature for dynamic focusing. We investigated the effect of change of the mirror curvature to conclude that the amount of spot shifting is only determined by tip or tilt term of the Zernike polynomial, which means that whatever curvature the deformable mirror takes we can use the relationship between tip, tilt amplitude and the amount of spot movement described in the previous paragraph.

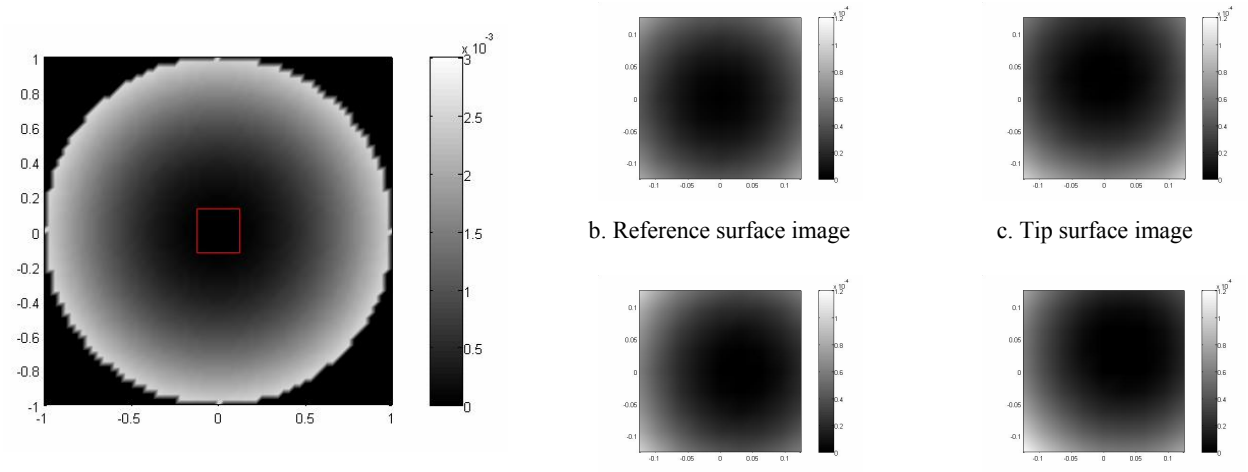

a. The reference image b. Reference surface image c. Tip surface image

d. Tilt surface image e. Tip tilt surface image

Fig. 4. Desired deformable mirror shapes to obtain shifted images

4.2 Experimental results

We used a USAF resolution target as an object to test our method. The image of the resolution target is shown in Fig. 5. The specified region is where we are interested in. To see the performance of our method, we deliberately reduced the sensor resolution by a factor of 2, i.e., we integrated neighboring four pixels to form a new pixel, and compared the super-resolution result with the real image taken by the camera. Fig.6 shows the real image of the specified area and Fig.7 show four different observations of reduced size.

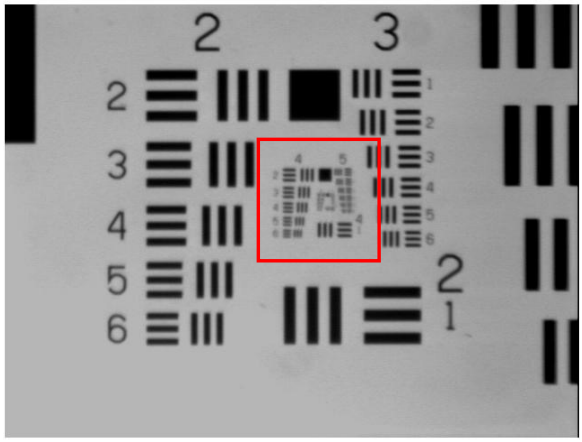

Fig. 5. The resolution target

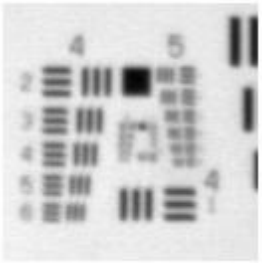

Fig. 6. Real image of the specified area

a. Reference image

b. Tip image

c. Tilt image

c. Tip-tilt image

Fig. 7. Reduced observations

The reference, tip, tilt, and tip-tilt image mean the images obtained when nothing, tip, tilt and both tip and tilt terms of Zernike polynomials were added to the reference shape of the deformable mirror, respectively. We calculated the required control signals to make desired mirror shape, using the influence matrix. For example, let us say $\mathbf{v}_{ref}$ denotes the control signal corresponding to the reference shape of the mirror. If our desired mirror shape is tip with amplitude 0.3, $\delta\mathbf{z}$ in Eq.1 becomes,

$$\delta\mathbf{z}_{tip} = \begin{bmatrix} 0.3 & 0 & \cdots & 0 \end{bmatrix}^T \tag{13}$$

and the control signal corresponding to tip mirror shape is,

$$\mathbf{v}_{tip} = \mathbf{A}^{+}\delta\mathbf{z}_{tip} + \mathbf{v}_{ref} \tag{14}$$

Likewise, when we want to make 'tilt' surface, then, $\delta\mathbf{z}_{tilt}$ becomes,

$$\delta\mathbf{z}_{tilt} = \begin{bmatrix} 0 & 0.3 & \cdots & 0 \end{bmatrix}^T \tag{15}$$

and we can calculate the control signal in similar manner.

After we obtained the four different observations, we applied the super-resolution algorithm described in section 3 using those images to synthesize high resolution image. The result is shown in Fig.8d. For comparison, the bilinear interpolated (a) and zero order hold expanded (b) images of the first observation (reference image) are shown together.

a. Bilinear interpolated

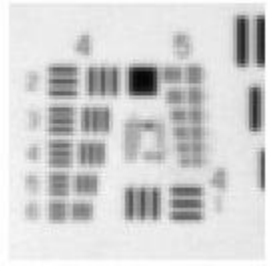

b. Zero order hold expanded

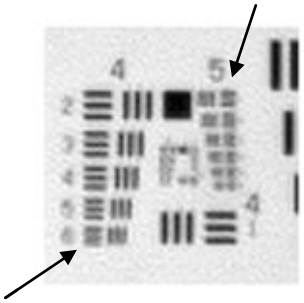

c. restored image without enhancing resolution

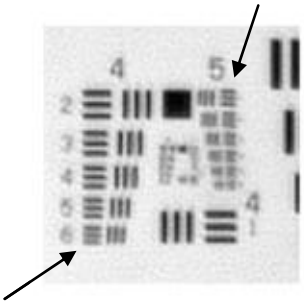

d. Super-resolved

Fig. 8. result

We can see that resolution of the synthesized image apparently enhanced compared to the each observations. The reconstructed image even seems better than the real image. That is because the super-resolution algorithm being used here does deblurring, i.e., image restoration together with enhancing resolution. To compare the result in the same condition, we performed restoration process to the bilinearly interpolated image. The result is shown in Fig.8c.

In the restored image, blurring reduced to the similar level of the super-resolved image in Fig.8d. However, the critical difference appears at the first element of the fifth group and the sixth element of the fourth group, which are indicated by the arrows. We can see that in both regions the three horizontal and vertical lines are resolved in the super-resolve image in Fig.8d, but not in the restored image in Fig.8c.

4.3 Parameters affecting the reconstruction performance

There are several algorithmic parameters in the super-resolution algorithm described in section3 such as the smoothening parameter λ and the discontinuity parameter h_0. To obtain the result shown in Fig.8d, we used $\lambda = 15$ and $h_0 = 1$. Usually, there is no general rule to determine these kinds of parameters. We investigate here the effect of each parameter change.

Fig.9 Shows the reconstructed images when λ changes from 10^{-10} to 10^{2}. h_0 was kept as one in this case. As mentioned in section 3, λ is related to smoothening, and the image is more smoothened when the value is smaller. As we expect, we can see that smaller λ value blurs the details in the figure. However, there is no more enhancement when λ is greater than 10^{-4}. Smoothness of the image is kept almost constant. This is because all the details resolvable in this

case are already isolated, that is, any intensity difference between neighboring pixels exceeding one is regarded meaningful and preserved. So even though the characteristic length defined in Eq.11 decreases more and more, there is no meaningful increase in resolution.

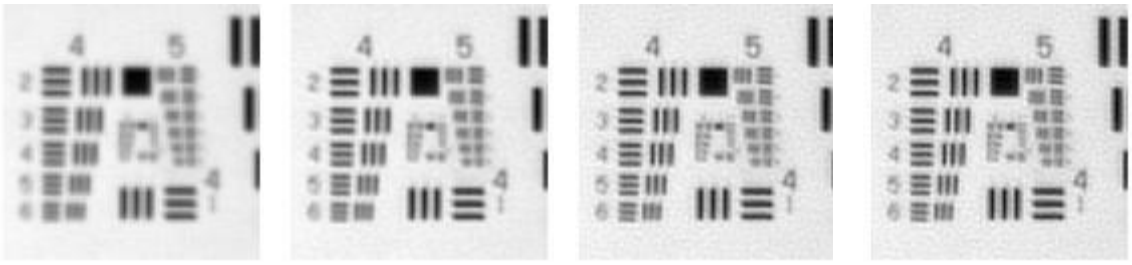

a. $\lambda = 10^{-10}$ b. $\lambda = 10^{-7}$ c. $\lambda = 10^{-4}$ d. $\lambda = 10^{2}$

Fig. 9. Effect of λ change ($h_0 = 1$)

To see the effect of h_0, we changed h_0 from 0.0001 to 2.0 keeping $\lambda = 10^{-10}$. As we can see in Fig.10a, b and c, the image becomes clearer as h_0 becomes smaller. We attribute this result to decrease of gradient limit defined in Eq.12 Although the characteristic length is large when $\lambda = 10^{-10}$, small level of gradient can generate line field. Fig.9d and Fig.10c look almost identical. When we compare Fig.10c and d, however, further decrease of h_0 does not make the image clearer. This is also because the meaningful discontinuities in the image are already preserved.

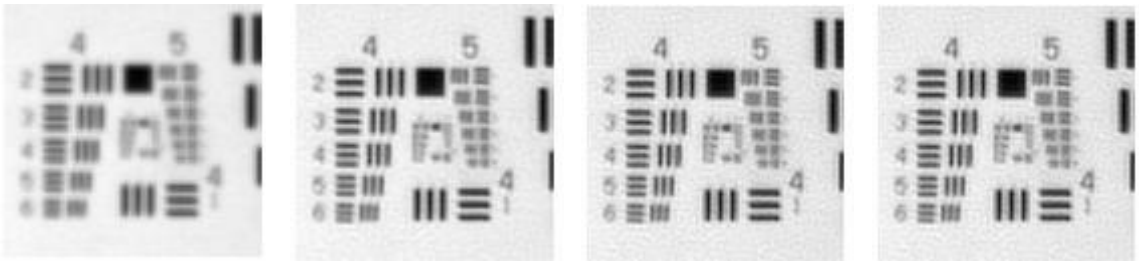

a. $h_0 = 2.0$ b. $h_0 = 0.05$ c. $h_0 = 0.01$ d. $h_0 = 0.0001$

Fig. 10. Effect of h_0 change ($\lambda = 10^{-10}$)

5. CONCLUSION

We proposed an active vision system using deformable mirror at the pupil plane. When we need a small amount of pupil plane modulation, deformable mirror is more advantageous than LC-SLM. Using this system and the suitable algorithm, we demonstrated that our active imaging system can enhance the resolution which is limited by CCD cell size. In the experimental study, we took four different sample images by adding the first order Zernike polynomial terms to the reference surface of the deformable mirror, and used them to synthesize a higher resolution image. By comparing the super-resolved image and restored image without super-resolution, we could say that the super resolution method does something more than simple restoration. We also analyzed the effect of the algorithmic parameters to see how they contribute the super-resolution algorithm. Super-resolution is one application that can be done by the proposed active vision system. We expect that when this super-resolution technique is combined with the other functionalities of the active vision system, such as dynamic focusing or aberration correction, we will be able to get high quality super-resolved image from the system.

REFERENCES

1. J. W. Goodman, *Introduction to Fourier Optics*, Roberts & Company, Colorado, 2005.
2. V. Laude, "Twisted-nematic liquid-crystal pixelated active lens", Opt. commun. 153, 134-152 (1998).
3. S. Park, M. Park, and M. Kang, "Super-Resolution Image Reconstruction: A Technical Overview", IEEE signal processing magazine, 21-36 (2003).
4. P. Luca, N. Piergiorgio, B. Oliviero, "A resolution improvement technique for two-dimensional detectors", SPIE3101, 83-94 (1997).
5. V. Laude, C. Dirson, "Liquid-crystal active lens: application to image resolution enhancement", Opt. commun. 163, 72-78 (1999).
6. G. Vdovin, P. M. Sarro and S. Middelhoek, "Technology and applications of micromachined adaptive mirrors", J. Micromech. Microeng. 9, R8-R20 (1999).
7. D. Rajan and S Chaudhuri, "An MRF-Based Approach to Generation of Super-Resolution Images from Blurred Observations", Journal of mathematical imaging and vision 16, 5-15 (2002).
8. G. Vdovin and P.M.Sarro, "Flexible mirror micromachined in silicon", Appl. opt. 34(16), 2968-2972 (1995).
9. M. Loktev, D. William, D. L. Monteiro and G. Vdovin, "Comparison study of the performance of piston, thin plate and membrane mirrors for correction of turbulence-induced phase distortions", Opt. commun. 192, 91-99 (2001).
10. M. Borm and E. Wolf, "Principles of Optics, Cambridge University, New York, 1999.
11. L. Zhu, P. Sun, D. Bartsch, W. R. Freeman, and Y. Fainman, "Adaptive control of a micromachined continuous-membrane deformable mirror for aberration compensation", Appl. opt. 38(1), 168-176 (1999)
12. S. Farsiu, D. Robinson, M. Elad and P. Milanfar, "Advances and Challenges in Super-Resolution", 2004 Wiley Periodicals, Inc. Vol.14, 47-57 (2004)
13. A. Blake and A. Zisserman, *Visual Reconstruction*, MIT press, Cambridge, 1987.